Experimental and theoretical verification of focusing in a large, periodically loaded transmission line negative refractive index metamaterial

Ashwin K. Iyer, Peter C. Kremer and George V. Eleftheriades

The Edward S. Rogers Sr. Department of Electrical and Computer Engineering, University of Toronto, Ontario, M5S 3G4, CANADA
gelefth@waves.utoronto.ca

http://www.waves.utoronto.ca/prof/gelefth/main.html

Abstract: We have previously shown that a new class of Negative Refractive Index (NRI) metamaterials can be constructed by periodically loading a host transmission line medium with inductors and capacitors in a dual (high-pass) configuration. A small planar NRI lens interfaced with a Positive Refractive Index (PRI) parallel-plate waveguide recently succeeded in demonstrating focusing of cylindrical waves. In this paper, we present theoretical and experimental data describing the focusing and dispersion characteristics of a significantly improved device that exhibits minimal edge effects, a larger NRI region permitting precise extraction of dispersion data, and a PRI region consisting of a microstrip grid, over which the fields may be observed. The experimentally obtained dispersion data exhibits excellent agreement with the theory predicted by periodic analysis, and depicts an extremely broadband region from 960MHz to 2.5GHz over which the refractive index remains negative. At the frequency at which the theory predicts a relative refractive index of –1, the measured field distribution shows a focal spot with a maximum beam width under one-half of a guide wavelength. These results are compared with field distributions obtained through mathematical simulations based on the plane-wave expansion technique, and exhibit a qualitative correspondence. The success of this experiment attests to the repeatability of the original experiment and affirms the viability of the transmission line approach to the design of NRI metamaterials.

OCIS codes: (100.3020) Image reconstruction-restoration; (110.2990) Image formation theory; (220.3630) Lenses; (070.2580) Fourier Optics; (350.4010) Microwaves

References and links

1. V. G. Veselago, "The electrodynamics of substances with simultaneously negative values of ε and μ," Sov. Phys. Usp. **10**, 509-514 (1968).
2. J. B. Pendry, A. J. Holden, D. J. Robins, W. J. Stewart, "Magnetism from conductors and enhanced nonlinear phenomena," IEEE Trans. on Microwave Theory and Tech. **47**, 2075-2084 (1999).
3. D. R. Smith, W. J. Padilla, D. C. Vier, S. C. Nemat-Nasser, S. Schultz, "Composite medium with simultaneously negative permeability and permittivity," Phys. Rev. Lett. **84**, 4184-4187 (2000).
4. R. A. Shelby, D. R. Smith, S. Schultz, "Experimental verification of a negative index of refraction," Science **292**, 77-79 (2001).
5. A. K. Iyer, G. V. Eleftheriades, "Negative refractive index metamaterials supporting 2-D waves," in MTT-S International Microwave Symposium Digest (Institute of Electrical and Electronics Engineers, Seattle, 2002) pp. 1067-1070.

#2056 - $15.00 US Received January 28, 2003; Revised March 25, 2003

6. G. V. Eleftheriades, A. K. Iyer, P. C. Kremer, "Planar negative refractive index media using periodically L-C loaded transmission lines," IEEE Trans. on Microwave Theory and Tech. **50**, 2702-2712 (2002).
7. A. Grbic, G. V. Eleftheriades, "A backward-wave antenna based on negative refractive index L-C networks," in IEEE Int. Symp. Ant. and Propag. (Institute of Electrical and Electronics Engineers, San Antonio, 2002) pp. 340-343.
8. A. Grbic, G. V. Eleftheriades, "Experimental verification of backward-wave radiation from a negative refractive index metamaterial," J. Appl. Phys. **92**, 5930-5935 (2002).
9. R. E. Collin, *Foundations for Microwave Engineering*, 2nd Ed. (McGraw-Hill, Inc., Toronto, 1992).
10. D. M. Pozar, *Microwave Engineering*, 2nd Ed. (John Wiley & Sons, Toronto, 1998).
11. J. B. Pendry, "Negative refraction makes a perfect lens," Phys. Rev. Lett. **85**, 3966-3969 (2000).
12. N. Fang, X. Zhang, "Imaging properties of a metamaterial superlens," in Proc. 2nd IEEE Conference on Nanotechnology (Institute of Electrical and Electronics Engineers, Washington D.C., 2002) pp. 225-228.
13. R. W. Ziolkowski, E. Heyman, "Wave propagation in media having negative permittivity and permeability," Phys. Rev. E **64**, 056625: 1-15.
14. I. V. Lindell, S. A. Tretyakov, K. I. Nikoskinen, S. Ilvonen, "BW media – media with negative parameters, capable of supporting backward waves," IEEE Micro. and Opt. Tech. Lett. **31**, 129-133 (2001).
15. J. A. Kong, B. Wu, Y. Zhang, "Lateral displacement of a Gaussian beam reflected from a grounded slab with negative permittivity and permeability," Appl. Phys. Lett. **80**, 2084-2086 (2002).
16. W. J. R. Hoefer, "The Transmission Line Matrix (TLM) Method," in *Numerical Techniques for Microwave and Millimeter-Wave Passive Structures*, T. Itoh, ed. (John Wiley & Sons, Toronto, 1989).
17. R. Ruppin, "Surface polaritons of a left-handed material slab," J. Phys.: Condens. Matter **13**, 1811-1819 (2001).

1. Introduction

It was V. G. Veselago who first proposed that materials possessing simultaneously negative magnetic permeability and electric permittivity are physically permissible and would exhibit a negative refractive index [1]. He termed these peculiar materials Left-Handed Media (LHM) because they support backward waves, for which **E**, **H**, and **k** form a left-handed triplet. Veselago postulated several interesting phenomena associated with LHM, including the reversal of conventional refraction, Cherenkov radiation, the Doppler shift, and the focusing of cylindrical waves at a planar interface using flat lenses. Interest in LHM was revived in 1999 when an artificial dielectric was designed and verified in experiment to exhibit negative material parameters giving rise to a negative effective refractive index at microwave frequencies [2-4]. These unusual artificial media, which we shall refer to as Negative Refractive Index (NRI) metamaterials, consist of an array of loosely coupled resonant cells, each consisting of thin wire strips and Split Ring-Resonators (SRRs), designed to possess a simultaneously negative permittivity and permeability, respectively. However, the explicit reliance on the split-ring resonance to synthesize a negative magnetic permeability makes these metamaterials inherently narrowband. In 2002, a different class of NRI metamaterials was introduced, based on the periodic reactive loading of a 2-D transmission line (TL) host medium in a dual (high-pass) configuration [5]. This approach to the design of NRI metamaterials offers several advantages: these structures do not utilize SRRs and are therefore inherently broadband; their unit cells are connected through a transmission line network and they may therefore be equipped with lumped elements, making them simultaneously scalable and compact; and they are truly planar.

A microstrip-based 55mm×30mm×1.5mm planar NRI lens interfaced with a parallel-plate waveguide was successful in experimentally verifying the focusing property predicted by Veselago [5,6]. Furthermore a fast version of this metamaterial (that is, one in which the phase velocity exceeds the speed of light in vacuum) was utilized to demonstrate backward-wave radiation from the fundamental Floquet mode, a phenomenon analogous to what Veselago termed "reversed Cherenkov radiation" [7,8]. In this paper, we present theoretical and experimental data describing the focusing and dispersion characteristics of a larger device consisting of a 105mm×200mm NRI lens interfaced with a 105mm×105mm Positive-Refractive-Index (PRI) medium, the latter of which is constructed using an unloaded microstrip grid. This new prototype offers significant improvements over the smaller structure originally used to verify focusing; specifically, the edge effects are minimized to more clearly

#2056 - $15.00 US Received January 28, 2003; Revised March 25, 2003

observe the attributes of the focal region; the increased size of the NRI region permits a closer observation of the spatial evolution of phase and therefore the extraction of more precise dispersion information; and the use of a microstrip grid instead of a parallel-plate waveguide enables the observation of the fields in the PRI region as well. The dispersion characteristics of the device are compared with the results of periodic analysis of microwave networks, and we attempt to predict the field distributions through mathematical simulations based on the plane-wave expansion technique.

2. Theory

In the long-wavelength regime, the permittivity and permeability of conventional materials can be artificially synthesized using periodic L-C networks arranged in a low-pass configuration. In the dual (high-pass) configuration, these equivalent material parameters assume simultaneously negative values, and may therefore be used to synthesize a negative refractive index [5-8]. Figure 1 illustrates the unit cell for the periodic, 2-D NRI structure, which consists of a host transmission line medium periodically loaded by discrete reactive elements.

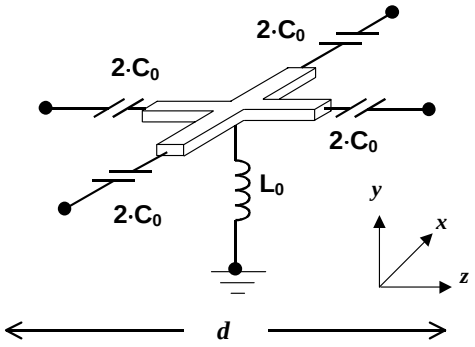

Fig. 1. Unit cell for the 2-D transmission line NRI metamaterial.

When the unit cell dimension d is much smaller than a wavelength, arrays of these unit cells may be viewed as homogeneous, effective media. The representation of a transmission-line network as an effective medium requires an appropriate mapping of voltages and currents **V** and **I**, related by the distributed capacitance and inductance of the transmission line, to the field quantities **E** and **H**, related by the material parameters of the effective medium. The predominance of a TM_y mode in these structures under the assumption of homogeneity justifies the equivalent material parameters,

$$\mu_N(\omega) = \mu_P - \frac{1/g}{\omega^2 C_0 d},\ \varepsilon_N(\omega) = \varepsilon_P - \frac{g}{\omega^2 L_0 d}. \tag{1}$$

Here μ_P and ε_P describe the intrinsic material parameters of the host transmission line medium, contributing positively to the equivalent parameters of the NRI medium, and the reactive inclusions C_0 and L_0 provide the desired negative contribution that diminishes with frequency ω. Of course, such a mapping from circuit to field quantities also entails the specific geometry of the transmission line, the effect of which is lumped into the parameter g of Eq. (1) through the ratio of the characteristic impedance of the transmission line to the intrinsic impedance of the bulk medium surrounding the network. Similar expressions were previously presented in [6,8], normalized with respect to the g parameter. The PRI parameters ε_P and μ_P may therefore be obtained from the per-unit-length capacitance C_x and inductance L_x of the transmission line segments comprising the host medium through the parameter g, according to Eq. (2):

#2056 - $15.00 US Received January 28, 2003; Revised March 25, 2003

$$\varepsilon_P = 2C_x \cdot g,\ \mu_P = L_x / g, \tag{2}$$

where the factor of two multiplying C_x is a correction factor in the extrapolation from one to two dimensions [6,8].

The equivalent material parameters of Eq. (1) may therefore be evaluated once the geometry, loading, and frequency are specified. The new experimental device is fabricated on a Rogers RT Duroid® 6002 ceramic (ε_r=2.94) substrate of height h=1.524mm (60mil) and consists of a PRI region measuring 21×21 cells (105mm×105mm), and an adjacent NRI region measuring 21×40 cells (105mm×200mm). Both the PRI medium, and the NRI host medium, consist of a square grid of w=400μm wide microstrip lines with d=5mm period, for which the distributed parameters and characteristic impedance may be obtained using standard quasi-static formulas [9,10], given in Eqs. (3)-(5).

$$\varepsilon_{eff} = \frac{\varepsilon_r + 1}{2} + \frac{\varepsilon_r - 1}{2}\sqrt{\frac{1}{1+12h/w}},\ \eta_{eff} = \frac{\eta_0}{\sqrt{\varepsilon_{eff}}},\ \eta_0 = 377\Omega \tag{3}$$

$$Z_0 = \eta_{eff}\, g, \quad g = \frac{1}{2\pi}\ln\left(\frac{8h}{w} + \frac{w}{4h}\right) \tag{4}$$

$$C_x = \frac{2\pi\varepsilon_0\varepsilon_{eff}}{\ln\left(\frac{8h}{w} + \frac{w}{4h}\right)} = \frac{\varepsilon_0\varepsilon_{eff}}{g},\ L_x = Z_0^2 \cdot C_x = \mu_0 g \tag{5}$$

Essentially, a homogeneous space is realized through the effective permittivity ε_{eff}, for which the intrinsic impedance may be represented as η_{eff}, and the per-unit-length capacitance C_x and inductance L_x are obtained through the microstrip characteristic impedance Z_0. Substituting the design values yields ε_{eff} = 2.11, g = 0.54419, $\varepsilon_P = 2\varepsilon_{eff}\varepsilon_0$ and $\mu_P = \mu_0$, where we remind the reader that ε_{eff} represents the effective permittivity surrounding a single microstrip line. In the NRI region, 5.6nH chip inductors are embedded (in shunt) into rectangular holes punched into the substrate at each cell site, and chip capacitors of 1pF are surface-mounted between gaps separating the cells. To maintain uniformity throughout, 2pF capacitors were placed at the array edges, followed by matching resistors.

It has been noted by various authors [1,6,11-13] that the condition of greatest interest to the problem of focusing in NRI metamaterials is that for which the relative refractive index (n_{REL}) at a planar interface between a PRI medium and NRI medium is –1. However, due to the dispersive nature of the equivalent material parameters of Eq. (1), this condition can only be satisfied at a particular frequency ω_0, as described by the equality

$$\sqrt{\mu_N(\omega_0)\varepsilon_N(\omega_0)} = \sqrt{\mu_P\varepsilon_P}\,. \tag{6}$$

Thus, for transmission line NRI media, this frequency is specified as

$$\omega_0 = \left(L_0 \cdot \frac{2\varepsilon_{eff}\varepsilon_0 d}{g} + C_0 \cdot g\mu_0 d\right)^{-1/2}, \tag{7}$$

which is calculated using the design parameters to be ω_0=2π×2.18GHz.

We note that the problem of *perfect* focusing is far more stringent, requiring that the PRI and NRI media be impedance matched at ω_0 such that $\mu_N(\omega_0) = -\mu_P$ and $\varepsilon_N(\omega_0) = -\varepsilon_P$. Many researchers have also noted the extreme sensitivity of this requirement, which may prove challenging for practical implementation (e.g., [12]). From the values chosen, it is apparent that we have relaxed this requirement so as to more easily investigate the salient features of focusing.

#2056 - $15.00 US Received January 28, 2003; Revised March 25, 2003

2.1 Dispersion characteristics

Periodic structures can be completely characterized by their dispersion characteristics, and standard procedures for the periodic analysis of one-dimensional microwave networks have been presented in such references as [9,10]. We employ these techniques to analyze the dispersion along a single row of cells in the NRI region, with the transmission line parameters appropriately modified to account for the two-dimensional nature of the structure. The propagation constant β is given by

$$\cos\beta d = \cos\theta - \frac{1}{2\omega^2 L_0 C_0}\cos^2\frac{\theta}{2} + \frac{1}{2\omega}\left(\frac{1}{C_0 Z_0} + \frac{1}{L_0 Y_0}\right)\sin\theta \tag{8}$$

where θ is the phase delay through the microstrip component of the cell, characterized by $\varepsilon_P = 2\varepsilon_{eff}\varepsilon_0$ and $\mu_P = \mu_0$, and Z_0 is the characteristic impedance of the microstrip lines, as given by Eq. (4). The propagation constant is also approximated by the equivalent material parameters of Eq. (1) through the relation

$$\beta = -\omega\sqrt{\mu_N(\omega_0)\varepsilon_N(\omega_0)}. \tag{9}$$

Figure 2 presents the NRI dispersion relation for the parameters of the present experiment, as predicted by Eq. (8) (dashed curve), and by Eq. (9) (solid curve), and illustrates the left-handed (LH) nature of the NRI medium in the first passband.

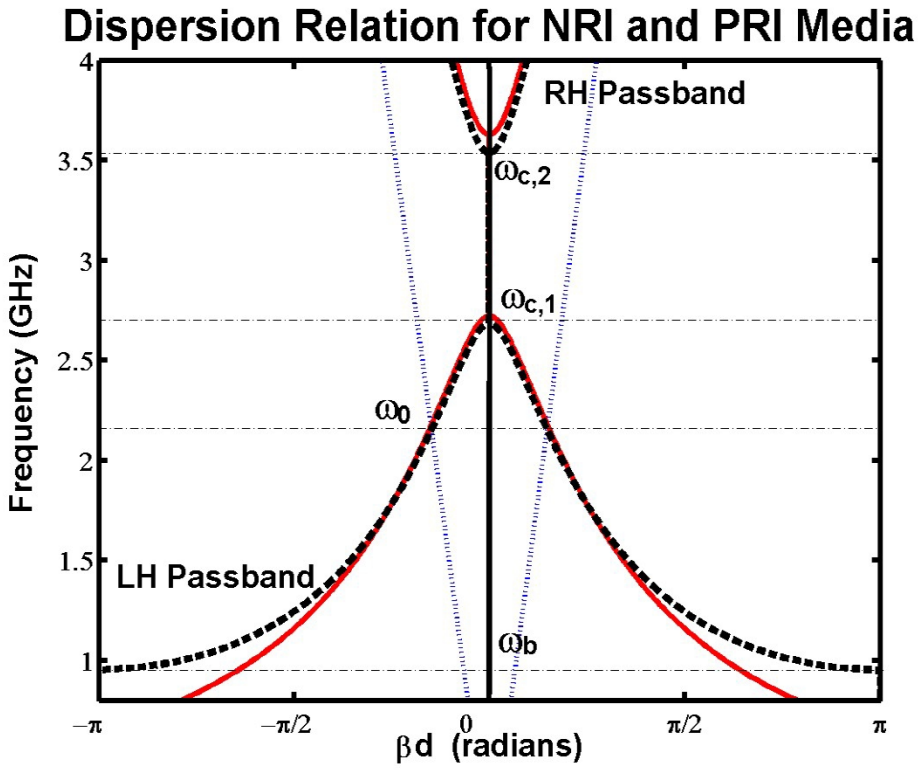

Fig. 2. Dispersion relation for designed NRI medium as obtained through periodic analysis (dashed curve) and using the equivalent material parameters (solid curve), and dispersion relation for PRI medium (dotted curve). The NRI dispersion curves indicate a Left-Handed (LH) passband enclosed by the Bragg frequency ω_b and stopband cutoffs $\omega_{C,1}$ and $\omega_{C,2}$, and the intersection of the NRI and PRI dispersion curves indicate the frequency ω_0 at which n_{REL}=–1.

#2056 - $15.00 US
Received January 28, 2003; Revised March 25, 2003

The lowest cut-off (Bragg) frequency is followed by a passband exhibiting a distinct backward wave characteristic [5,14], a stopband, and a higher-order band possessing a right-handed (RH) characteristic. The Bragg frequency is approximately given by the solution to Eq. (8) when $\beta d = \pi$, described by the following quadratic equation:

$$A\omega_b^4 + B\omega_b^2 + 1 = 0,$$
$$A = L_0 C_0 \mu_P \varepsilon_P d^2,\ B = -(L_0 \frac{\varepsilon_P d}{g} + C_0 g \mu_P d + 4 L_0 C_0), \tag{10}$$

yielding $\omega_b = 2\pi\times960$MHz. Near the Bragg frequency, the phase delay through the transmission line component of the unit cell, θ, becomes small, and the solution is approximated by [6]

$$\omega_b = \frac{1}{2\sqrt{L_0 C_0}}. \tag{11}$$

It is evident from Eq. (1) that the equivalent material parameter expressions, obtained from the periodic analysis under the assumption of homogeneity (βd small), cannot predict the existence of this Bragg condition, and the associated dispersion curve diverges as $\omega\to0$. Consequently, the validity of Eq. (1) is limited to the interior LH region, before the stopband. The cutoff frequencies for the first stopband, however, are predicted both by Eq. (8) and Eq. (1), and are approximately given by [6]

$$\omega_{c,1} = \sqrt{\frac{1}{C_0 g \mu_P d}},\quad \omega_{c,2} = \sqrt{\frac{1}{L_0 \frac{\varepsilon_P d}{g}}}, \tag{12}$$

yielding $\omega_{C,1}=2\pi\times2.72$GHz and $\omega_{C,2}=2\pi\times3.63$GHz, respectively. Figure 2 also illustrates the dispersion of the PRI medium (dotted curve), which intersects the NRI dispersion curve near $\omega_0=2\pi\times2.18$GHz, where it was predicted by Eqs. (6) and (7) that the condition $n_{REL} = -1$ would be encountered.

2.2 Plane-wave expansion analysis

In order to compare the new experimental results with theory, we employ a technique based on the plane-wave expansion to examine a homogeneous PRI/NRI interface excited by an infinitesimal line source oriented vertically to the device plane; this is equivalent to determining the corresponding Green's function. This method has been previously employed by Kong *et al*. [15] to describe the refraction of a Gaussian beam through a medium with negative material parameters. The arrangement presently studied consists of a NRI material slab embedded between two semi-infinite half-spaces, and is depicted in Fig. 3. The NRI material of thickness d_N is placed at $x=d_S$ and excited by a vertical (y-directed) line source located at $x=z=0$ inside a PRI medium. For $n_{REL} = -1$, the focal plane is located at $x=2\cdot d_S$. The resistive terminations Z_{term} to the right of the NRI material are modeled by a third medium with positive parameters $\mu_T=\mu_0$ and $\varepsilon_T=\varepsilon_{term}\varepsilon_0$, where $\varepsilon_{term}=(\eta_0/Z_{term})^2$, and all media are considered infinite in the transverse z-direction. The plane-wave expansion method is then used to solve the problem of Fig. 3.

#2056 - $15.00 US Received January 28, 2003; Revised March 25, 2003

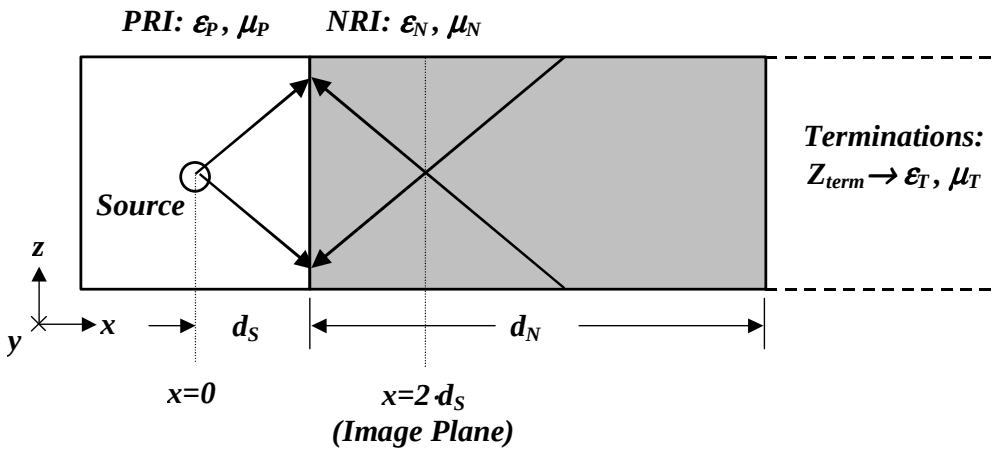

Fig. 3. PRI/NRI metamaterial interface examined by the plane-wave expansion theory. The arrows depict the wavevectors in each medium.

The fields in each medium i={P,N,T} are represented as follows (note: a positive time-harmonic variation of the form $\exp(j\omega t)$ is assumed):

$$E_{y,i}(x,z) = \frac{1}{2\pi} \int_{-\infty}^{\infty} \tilde{E}_{y,i}(x,k_{x,i}) e^{-jk_{z,i}z} dk_{z,i}, \tag{13}$$

$$k_{x,i} = \pm j\sqrt{k_{z,i}^2 - k_i^2}, \;\; k_i^2 = \omega^2 \varepsilon_i \mu_i. \tag{14}$$

Equation (14) describes the dispersion of material i, and the positive root is chosen only for the NRI metamaterial. The resulting expression for the spectral components of the y-directed electric field in the NRI metamaterial is

$$\tilde{E}_{y,N} = 2\tilde{E}_{y,P}\Big|_{x=0} e^{-jk_{x,P}d_S} \left\{ \frac{(\tau_B+1)e^{-jk_{x,N}(x-(d_S+d_N))} + (\tau_B-1)e^{+jk_{x,N}(x-(d_S+d_N))}}{(\tau_A+1)(\tau_B+1)e^{+jk_{x,N}d_N} - (\tau_A-1)(\tau_B-1)e^{-jk_{x,N}d_N}} \right\} \tag{15}$$

where

$$\tau_A = \frac{k_{x,N}\mu_P}{k_{x,P}\mu_N}, \quad \tau_B = \frac{k_{x,N}\mu_T}{k_{x,T}\mu_N}, \quad \tilde{E}_{y,P}\Big|_{x=0} = -\frac{\omega\mu_P}{2k_{x,P}}. \tag{16}$$

The commercial mathematical package Matlab® was employed to compute the fields as given by Eqs. (10)–(13), supplemented by the design parameters, with the source a distance of d_S = 10 cells from the interface. Figure 4 shows the resulting vertical electric field magnitude and phase distributions at $\omega_0 = 2\pi \times 2.18$GHz, the frequency at which Eqs. (6) and (7) predict $n_{REL} = -1$.

#2056 - $15.00 US
Received January 28, 2003; Revised March 25, 2003

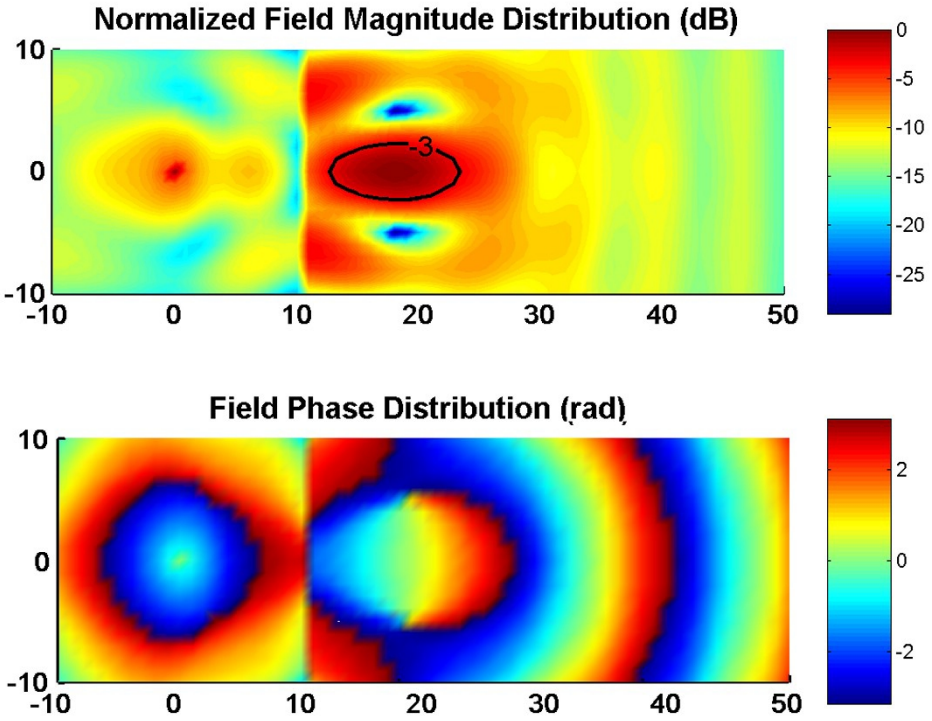

Fig. 4. Vertical electric field distribution over a PRI/NRI interface (PRI: cells –10 to 10, NRI: cells 11 to 50) predicted by plane-wave expansion analysis at 2.18GHz (normalized individually in the PRI and NRI regions to their maximum respective amplitudes) illustrating focusing

Before interpreting the results, it should be noted that, due to the representation of the source as an infinitesimal line source in an infinite medium, the relative transmission from source to focal plane is not representative of the actual transmission in a planar device. Therefore, the field magnitudes shown in Fig. 4 have been normalized individually in the PRI and NRI regions to their maximum respective values.

From Fig. 4, focusing is evident in both the increased transmission and confinement of the fields near the focal plane (x=2·d_S = cell 20), which have been indicated by a contour at the –3dB level in the NRI medium, and the reversal of the concavity of the phase-fronts at the interface and at the focal plane. Although focusing is apparent, these results do not suggest *perfect* focusing, since the PRI and NRI media are not impedance-matched at ω_0. That is, while $\mu_N(\omega_0)\varepsilon_N(\omega_0) = \varepsilon_P\mu_P$ at 2.18GHz (the $n_{REL} = -1$ condition), the material parameters have not been individually synthesized such that $\mu_N(\omega_0) = -\mu_P$ and $\varepsilon_N(\omega_0) = -\varepsilon_P$, resulting in a beam characteristic similar to the results reported in [13]. We note that $\mu_N(\omega_0)$ and $\varepsilon_N(\omega_0)$ can be individually synthesized to meet this constraint through the proper selection of the reactive inclusions L_0 and C_0 in Eq. (1); however, the precision with which this is achieved is limited by device and process tolerances.

#2056 - $15.00 US
Received January 28, 2003; Revised March 25, 2003

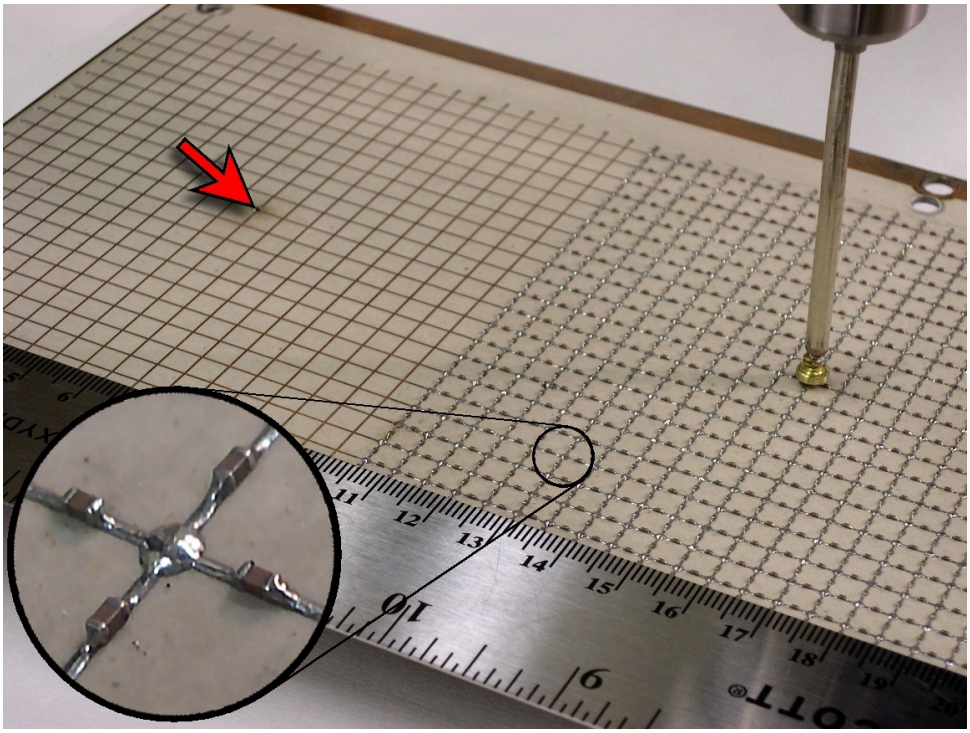

Fig. 5. Experimental prototype. The PRI region measures 21×21 cells (105mm×105mm), and the adjacent NRI region measures 21×40 cells (105mm×200mm). The inset magnifies a single NRI unit cell, consisting of a microstrip grid loaded with surface-mounted capacitors and an inductor embedded into the substrate at the central node. The near-field detecting probe is also depicted, and the arrow indicates the location of the vertical excitation probe.

3. Experiment

The new experimental device measures approximately 105mm×305mm×1.5mm and is shown in Fig. 5. Also shown in the inset is a magnification of a single NRI unit cell, consisting of a microstrip grid loaded with surface-mounted capacitors (in series) and an inductor embedded into the substrate (in shunt) at the central node, similar to the schematic presented in Fig. 1. The corresponding PRI unit cell consists of the microstrip grid alone. An HP8753D vector network analyzer was employed to take transmission scattering parameter readings from 0.8–4GHz at 8MHz intervals at each unit cell calibrated at the inductor sites. Port 1 of the analyzer provided the excitation via a shorted SMA (coaxial) connector placed in the center of the PRI region, and port 2 was connected to a near-field coaxial probe (depicted in Fig. 5) that was scanned over the surface of the PRI and NRI regions using a stepper motor. The probe was designed to measure the vertical electric fields through capacitive coupling at a distance of approximately 0.5mm from the device plane.

The dispersion characteristic of the NRI medium was obtained from the experimental data using the average phase shift incurred per unit cell (βd) along the central row (row 11) of the device, and is presented in Fig. 6 (only the LH passband is depicted; the experimental data within the stopband, and the subsequent higher-order band, is obscured due to strong mismatch losses at these frequencies). This dispersion relation reveals a well-defined region of backward-wave propagation extending from the Bragg frequency (960MHz) to approximately 2.5GHz that exhibits a distinct NRI characteristic [5,6], largely in excellent agreement with that predicted by periodic analysis of the corresponding infinite structure presented in Fig. 2 (also depicted in Fig. 6 for ease of comparison).

#2056 - $15.00 US Received January 28, 2003; Revised March 25, 2003

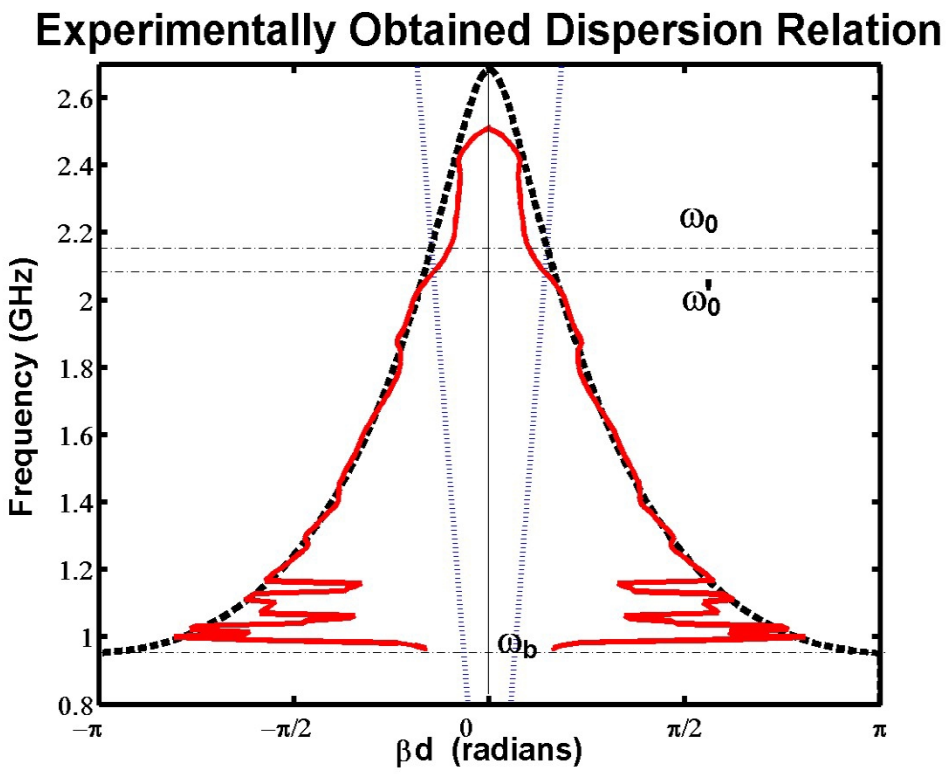

Fig. 6. Experimentally obtained NRI dispersion relation (solid curve) indicating the Bragg frequency at 960MHz and a well-defined NRI region extending to approximately 2.5GHz (data obtained for region $\beta d=-\pi$ to $\beta d=0$ and reflected in the $\beta d=0$ axis for the space-reversed solution). Also depicted are the theoretical NRI (dashed curve) and PRI (dotted curve) dispersion relations. The intersection of the PRI dispersion with the experimental NRI dispersion at ω'_0 differs slightly from the predicted intersection at ω_b.

The minor fluctuations near the Bragg frequency result from the fact that the guide wavelength in these NRI media varies proportionally, and not inversely, with frequency; consequently, at low frequencies, the guided waves experience the coarseness of the transmission line grid and the assumption of homogeneity begins to break down. Accordingly, phase measurements taken at finite intervals (d=5mm in the present case) often do not adequately sample the rapidly varying phase at these frequencies. The dispersion data of Fig. 6 indicates that this phenomenon becomes evident near 1.17GHz, where the guide wavelength is calculated to be 17.4mm, roughly equal to 3.5d. Reference [16] has investigated the issue of granularity in the context of the transmission line method (TLM), and describes a similar cutoff of $\lambda=4d$.

The effective refractive index can be computed from the dispersion data as $n=\phi c/\omega d$, where c is the speed of light in vacuum and ϕ is the measured average phase shift per unit cell βd. In the most well defined region from 1.17GHz to 2.03GHz, the absolute refractive index ranges from approximately –14.76 to –2.63. Since the PRI region is expected to possess an absolute refractive index of $\sqrt{(2\cdot\varepsilon_{eff})}=+2.05$, the corresponding relative refractive index n_{REL} varies from approximately –7.20 to –1.28. Using Eqs. (6) and (7), it was predicted that the device would encounter the condition $n_{REL}=-1$ near $\omega_0=2\pi\times2.18$GHz, which is indicated in Fig. 6 at the intersection between the theoretical NRI and PRI dispersion curves. However, this condition is achieved earlier, near $\omega'_0=2\pi\times2.09$ GHz, approximately where the experimental NRI dispersion curve intersects with the theoretical PRI dispersion curve.

#2056 - $15.00 US Received January 28, 2003; Revised March 25, 2003

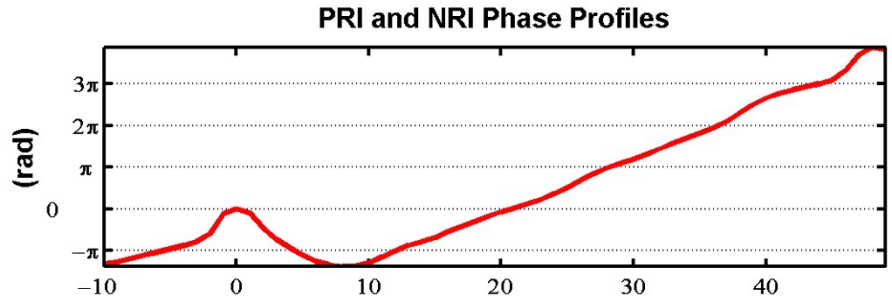

Fig. 7. Experimental data showing phase profile in the PRI and NRI regions (PRI: cells –10 to 10, NRI: cells 11 to 50) along the central row of the experimental device at 2.09GHz

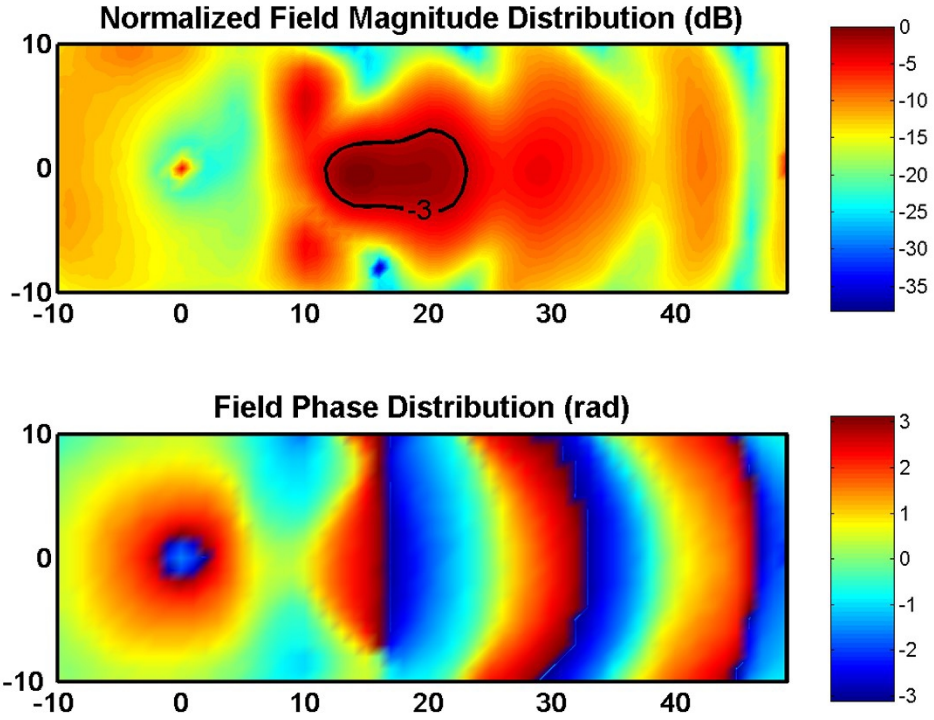

Fig. 8. Experimental data showing field magnitude and phase distributions in PRI and NRI regions at 2.09GHz (PRI: cells –10 to 10, NRI: cells 11 to 50). (1.68MB_movie showing experimental field magnitude distributions from 1.0GHz to 2.5GHz; 1.62MB movie showing experimental field phase distributions from 1.0GHz to 2.5GHz).

This is illustrated by Fig. 7, which depicts the measured phase profiles in the PRI and NRI regions along the central row of the experimental device, containing the source. The distinction between phase lag in the PRI medium and phase advance in the NRI medium is apparent; furthermore, the relative index can be inferred from the slopes of the two profiles, which are nearly equal at this frequency, suggesting $n_{REL} = -1$. Giving further credibility to this observation is the fact that the absolute phase at the source plane (cell 0) is almost exactly restored at the image plane (cell 20) at this frequency. The magnitude and phase of the

#2056 - $15.00 US
Received January 28, 2003; Revised March 25, 2003

measured vertical electric fields over the structure at 2.09GHz are depicted in Fig. 8. The increased transmission at the focal plane, as well as the convergent progression of the wavefronts of Fig. 8 are indicative of focusing, and exhibit a qualitative correspondence with the field distribution at 2.18GHz predicted by the plane-wave expansion analysis (Fig. 4). The phase distributions between the two results, however, exhibit some discrepancy, which may be attributed to the many levels of simplification inherent in the plane-wave expansion theory used. Specifically, the theory employs homogeneous media in a purely two-dimensional geometry (i.e., infinite in the *y*- and *z*-directions of Fig. 3), and therefore cannot account for the effect of periodicity, grid truncation, termination, and planar confinement evident in the experimental results. Moreover, the phase suffers from a greater sensitivity to these conditions than does the magnitude. However, at their respective frequencies, the phase distributions of the experiment and theory reveal guide wavelengths that are approximately equal ($\lambda_{\mathrm{NRI,experiment}}$=70mm and $\lambda_{\mathrm{NRI,theory}}$=67.6mm). Consequently, the beam widths of Fig. 4 and Fig. 8 at the –3dB level may be compared; the maximum beam widths in millimeters are found to be 32mm in experiment and 23mm in the theory, corresponding to $0.46\lambda_{\mathrm{NRI,experiment}}$ and $0.34\lambda_{\mathrm{NRI,\ theory}}$, respectively.

The experimentally obtained field distributions also indicate what seem to be surface-wave effects at the PRI/NRI boundary that appear near, and persist well beyond, ω'_0. These phenomena are reminiscent of the surface modes described by Ruppin [17] and Pendry [2,11], which vary exponentially away from the PRI/NRI interface.

At 2.4GHz, the dispersion data appears to undergo a steep approach towards a stopband at 2.5GHz. It is interesting to note that the *absolute* refractive index at 2.4GHz is almost exactly –1, suggesting the strong possibility that in this frequency region, extending into the impending stopband, fast waves are excited at the NRI-air surface boundary, and the structure radiates. The entire region over which the refractive index remains negative, from approximately 960MHz to 2.5GHz, corresponds to a bandwidth that may be conservatively placed at 85%.

The behaviour of the field distribution as the frequency is varied also exhibits characteristics typical of NRI focusing. The two animations associated with Fig. 8 present the measured field magnitude and phase distributions, respectively, over the PRI and NRI regions as the frequency is varied. Transmission from the PRI region into the NRI region increases steadily beyond the Bragg frequency, and the first evidence of a focused beam becomes apparent near 1.3GHz. At this frequency, the PRI and NRI regions exhibit distinct phase lag and phase advance characteristics, respectively, similar to the behaviour illustrated in Fig. 7, and as the frequency is increased, the phase distribution indicates a steadily increasing guide wavelength. Near 1.8GHz the transmission near the focal plane increases, and near 2GHz, where, according to the dispersion data, it is expected the device will encounter the condition $n_{REL} = -1$, the focus appears. The focal spot recedes slowly to the interface as the frequency is increased, a phenomenon predicted by geometrical optics for NRI media [6], and contrary to that observed for conventional media. Beyond the stopband edge near 2.5GHz, the phase exhibits a near-zero progression, and transmission into the NRI region is weak.

4. Conclusion

We have presented experimental and theoretical data describing the focusing and dispersion characteristics of a 105mm×305mm transmission line-based NRI focusing device. The experimentally obtained dispersion data exhibits excellent agreement with the theory predicted by periodic analysis, and depicts an extremely broadband region from 960MHz to 2.5GHz over which the refractive index remains negative. At 2.09GHz, close to the frequency at which the theory predicts a relative refractive index of –1, the focal spot has a maximum beam width under one-half of a guide wavelength, and exhibits a qualitative correspondence with the field distribution predicted by plane-wave expansion analysis.

#2056 - $15.00 US Received January 28, 2003; Revised March 25, 2003

Acknowledgments

This work was partly supported by the National Sciences and Engineering Research Council of Canada through Discovery and Strategic grants.

#2056 - $15.00 US Received January 28, 2003; Revised March 25, 2003